Electron Delocalization in the Radical Cation of 1,3,6,8-Tetraazatricyclo[4.4.1.1 3,8]dodecane, a 4-Nitrogen-7-Electron System

ARTICLE *in* JOURNAL OF THE AMERICAN CHEMICAL SOCIETY · FEBRUARY 2002

Impact Factor: 12.11 · DOI: 10.1021/ja016999n · Source: PubMed

12 AUTHORS, INCLUDING:

Albert M Brouwer
University of Amsterdam
143 PUBLICATIONS **3,347** CITATIONS
SEE PROFILE

Tamas Keszthelyi
Hungarian Academy of Sciences
36 PUBLICATIONS **415** CITATIONS
SEE PROFILE

Gurusamy Balakrishnan
University of Washington Seattle
53 PUBLICATIONS **950** CITATIONS
SEE PROFILE

Stephen F Nelsen
University of Wisconsin–Madison
118 PUBLICATIONS **2,220** CITATIONS
SEE PROFILE

J|A|C|S
ARTICLES
Published on Web 12/13/2001

Electron Delocalization in the Radical Cation of 1,3,6,8-Tetraazatricyclo[4.4.1.1^{3,8}]dodecane, a 4-Nitrogen-7-Electron System

Jurriaan M. Zwier,[†] Albert M. Brouwer,*[,†] Tamás Keszthelyi,[‡,||] Gurusamy Balakrishnan,[‡,#] Jesper F. Offersgaard,[▽,‡] Robert Wilbrandt,[⊗,‡] Frédérique Barbosa,[§] Urs Buser,[§] Jérôme Amaudrut,[§] Georg Gescheidt,*[,§] Stephen F. Nelsen,[⊥] and Charles D. Little[⊥]

Contribution from the Institute of Molecular Chemistry, University of Amsterdam, Nieuwe Achtergracht 129, NL-1018 WS Amsterdam, The Netherlands, Condensed Matter Physics and Chemistry Department, Risø National Laboratory, 4000 Roskilde, Denmark, Institute of Physical Chemistry, University Basel, Klingelbergstrasse 80, CH-4056 Basel, Switzerland, and Department of Chemistry, University of Wisconsin, 1101 University Avenue, Madison, Wisconsin 53706-1396

Received September 4, 2001

Abstract: The radical cation of 1,3,6,8-tetraazatricyclo [4.4.1.1^{3,8}]dodecane (TTD) has been studied using magnetic resonance and optical spectroscopic methods and computational techniques. With the help of deuterated isotopomers, assignments of EPR and resonance Raman spectra could be unequivocally established. The results demonstrate that the radical cation has D_{2d} symmetry, and instantaneous electron delocalization over the four equivalent nitrogen atoms occurs. This extensive delocalization in a completely saturated system is a unique feature of the TTD radical cation. The spectroscopy of TTD, in contrast to that of simpler diamines such as 1,4-diaza[2.2.2]bicyclooctane, simultaneously reveals the consequences of orbital interactions through space and through bonds. The relationship between nitrogen pyramidalization and hyperfine coupling constants in nitrogen-centered radical cations with a number of different bonding arrangements is reviewed.

1. Introduction

McKinney and Geske discovered the remarkable kinetic stability of the radical cation of 1,4-diazabicyclo[2.2.2]octane (DABCO, **1**, Chart 1) and discussed its EPR spectrum, which shows 2 equivalent nitrogens and 12 equivalent hydrogens, in terms of rapidly equilibrating single nitrogen-centered radical cations.[1] Hoffmann's elegant theoretical formulation of the concepts of orbital interactions through bond versus through space led to the realization that $\mathbf{1}^{\bullet+}$ is a through-σ-bond delocalized species in which the nitrogen lone pair orbitals interact through the three aligned C−C σ-bonds.[2,3] Heilbronner and Muszkat demonstrated on the basis of the vibronic structure in the photoelectron spectrum (PES) of **1** that its highest occupied molecular orbital (HOMO) has the a_2'' symmetry that is required by this description.[4] Subsequently, in the 1970s, several studies were conducted that were aimed at finding other examples of radical cations stabilized by through-bond interactions. Most radical cations of alkylamines decompose rapidly in room-temperature solutions, which leads to irreversible waves in cyclic voltammetry (CV) experiments.[5] DABCO, on the other hand, shows a re-reduction wave in the CV experiment, and an ESR signal of the radical cation can be readily observed at room

Chart 1

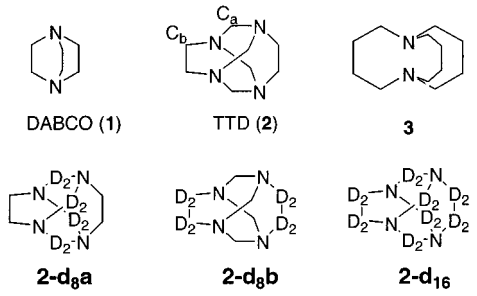

* To whom correspondence should be addressed. E-mail for A.M.B.: fred@science.uva.nl. E-mail for G.G.: Georg.Gescheidt@unibas.ch.
[†] University of Amsterdam.
[‡] Risø National Laboratory.
[§] University Basel.
[⊥] University of Wisconsin.
[||] Present address: Surface Spectroscopy Group, Chemical Research Center, P.O. Box 17, H-1525 Budapest, Hungary.
[#] Present address: Department of Chemistry, Princeton University, Princeton, NJ 08544-1009.
[▽] Present address: Delta Light and Optics, Hjortekærsvej 99, DK-2800 Lyngby, Denmark.
[⊗] Present address: Bornholms Amtsgymnasium, Søborgstræde 2, 3700 Rønne, Denmark.

(1) McKinney, T. M.; Geske, D. H. *J. Am. Chem. Soc.* **1965**, *87*, 3013−3014.
(2) Hoffmann, R.; Imamura, A.; Hehre, W. J. *J. Am. Chem. Soc.* **1968**, *90*, 1499.
(3) Hoffmann, R. *Acc. Chem. Res.* **1971**, *4*, 1.
(4) Heilbronner, E.; Muszkat, K. A. *J. Am. Chem. Soc.* **1970**, *92*, 3818−3821.
(5) Lindsay Smith, J. R.; Masheder, D. *J. Chem. Soc., Perkin Trans. 2* **1977**, 1732.

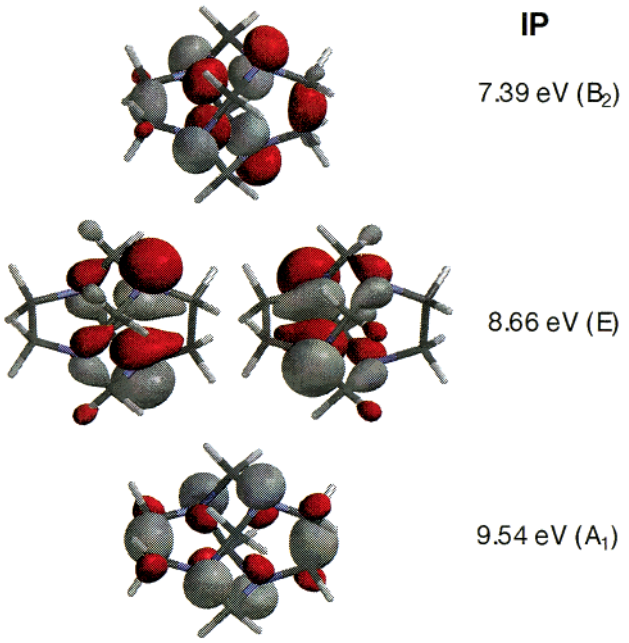

Figure 1. The four highest occupied molecular orbitals of TTD **2** (D_{2d} symmetry). Experimental values of the ionization potentials (IP) are given.[12]

temperature. Among the tertiary alkylamines that also showed a re-reduction wave were 1,3,6,8-tetraazatricyclo[4.4.1.1^{3,8}]-dodecane (TTD, **2**)[6−8] and 1,6-diazatricyclo[4.4.4]dodecane **3** (Chart 1).[9,10] As much as DABCO is a prototype molecule for through-bond interaction, **3**$^{\bullet+}$ is a classical example of direct interaction between nitrogen lone pair orbitals through space. It is the purpose of the present paper to definitively establish the bonding situation in the radical cation of TTD, in which through-space and through-bond interactions both play a role.

TTD has effective D_{2d} symmetry, as shown by its X-ray structure.[11] There are only two types of carbons (labeled a and b in the structure shown in Chart 1), which led to the correct assignment of its structure by means of NMR spectroscopy 72 years after it was first reported.[7,8] On the basis of quantum chemical calculations, the HOMO of TTD was assigned b_2 symmetry. The observed energy gap between the HOMO and the second highest occupied orbital (HOMO-1) is 1.27 eV, somewhat smaller than that in DABCO (2.1 eV).[12] The ab initio computed HOMOs are depicted in Figure 1, together with the experimental ionization energies.

The radical cation of TTD (**2**$^{\bullet+}$), unfortunately, could not be isolated in a stable crystalline form, but it could be studied by EPR spectroscopy. The observed hyperfine coupling constants (hfc's) were found to be in agreement with an average D_{2d} symmetric structure, but the large hyperfine interactions of the C_a hydrogens were considered to be unreasonable for the expected $^2B_2$ state, in which the two nitrogens neighboring the C_a carbon carry opposite spin density.[12] Nelsen and Buschek initially suggested that an inversion between the ^2E and $^2B_2$ states occurred upon ionization.[12] Haselbach and Nelsen et al. later proposed that distortion occurs to a structure of C_{2v} symmetry, with the charge instantaneously localized on one NCH_2CH_2N unit, in which interaction through space is possible.[13,14] This interpretation was supported by semiempirical quantum chemical calculations, but these are not reliable enough to be convincing. Therefore, stronger computational and experimental evidence for the structure of TTD$^{\bullet+}$ was sought.

The present paper will address the instantaneous spin distribution in the radical cation of TTD, which we (re)-investigated by means of EPR and ENDOR, (simultaneous) electronic absorption (SEOS),[15] and resonance Raman spectroscopy. To corroborate the assignment of the hfc's and the vibrational transitions established for **2**$^{\bullet+}$, deuterated derivatives **2-d$_8$a**, **2-d$_8$b**, and **2-d$_{16}$** were studied. The experimental results will be compared to theoretical predictions obtained by quantum mechanical calculations in order to achieve a consistent picture of the geometrical and electronic structure of TTD$^{\bullet+}$. We will demonstrate that the TTD radical cation has a single energy minimum with D_{2d} symmetry, and consequently the unpaired spin density is fully delocalized over the four amino groups. In an accompanying paper, the structure and spectroscopy of the neutral molecule are discussed. Although this molecule was previously believed to have D_{2d} symmetry,[11] the energy minimum actually occurs for an S_4 structure. The D_{2d} geometry corresponds to a transition structure on the interconversion pathway connecting two equivalent S_4 forms.[16]

2. Experimental Section

Synthesis. TTD was synthesized from formaldehyde and diaminoethane as described in the literature.[7] The isotopomers were obtained using the appropriately deuterated precursors. Diaminoethane-1,1,2,2-d_4 was a gift from Merck Sharp and Dohme.

EPR and SEOS Spectra. Oxidation of TTD was achieved by reaction with tris(4-bromophenyl)aminium hexachloroantimonate in CH_2Cl_2 under high vacuum (the samples were degassed by three pump−thaw cycles and kept under ca. 10^{-5} Torr). EPR spectra were taken on a Varian E9 spectrometer equipped with a data system (EWWIN, Scientific Software Services, Normal, IL). On the same instrument, SEOS spectra were taken with the use of an optical fiber diode array spectrometer (TIDAS, J&M, Aalen, Germany). ENDOR spectra were recorded on a BRUKER ESP 300 instrument.

Time-Resolved Optical Absorption Spectra. The radical cation of TTD in acetonitrile was generated with a cosensitization method.[17,18] The electron acceptor 1,4-dicyanonaphthalene (0.01 M) was excited at 355 nm (Spectra Physics Quanta Ray GCR-3 Nd:YAG laser) and allowed to react with biphenyl (0.2 M). The radical cation of the latter served to oxidize TTD (0.0005 M). After several hundred nanoseconds, the only detectable species in the transient absorption spectrum is TTD$^{\bullet+}$ (EG&G flashlamp FX-504, Princeton Instruments gated optical multichannel analyzer). This species decays on the time scale of microseconds by charge recombination with the reducing equivalent probably present as $O_2^{\bullet-}$. As a result, the chemical system is quite photostable:

(6) Nelsen, S. F.; Hintz, P. J. *J. Am. Chem. Soc.* **1972**, *94*, 7114−7117.
(7) Bischoff, C. A. *Chem. Ber.* **1898**, *31*, 3248.
(8) Volpp, G. *Chem. Ber.* **1962**, *95*, 1493.
(9) Alder, R. W.; Arrowsmith, R. J.; Casson, A.; Sessions, R. B.; Heilbronner, E.; Kovac, B.; Huber, H.; Taagepera, M. *J. Am. Chem. Soc.* **1981**, *103*, 6137.
(10) Alder, R. W.; Orpen, A. G.; White, J. M. *J. Chem. Soc., Chem. Commun.* **1985**, 949−951.
(11) Murray-Rust, P. *J. Chem. Soc., Perkin Trans. 2* **1974**, 1136.
(12) Nelsen, S. F.; Buschek, J. M. *J. Am. Chem. Soc.* **1974**, *96*, 6424−6428.
(13) Nelsen, S. F.; Haselbach, E.; Gschwind, R.; Klemm, U.; Lanyova, S. *J. Am. Chem. Soc.* **1978**, *100*, 4367−4368.
(14) Haselbach, E.; Bally, T.; Gschwind, R.; Klemm, U.; Lanyova, Z. *Chemia* **1979**, *33*, 405.
(15) Gescheidt, G. *Rev. Sci. Instrum.* **1994**, *65*, 2145−2146.
(16) Zwier, J. M.; Brouwer, A. M.; Buma, W. J.; Troisi, A.; Zerbetto, F. *J. Am. Chem. Soc.* **2002**, *124*, 149−158 (preceding paper in this issue).
(17) Mattes, S. L.; Farid, S. *J. Chem. Soc., Chem. Commun.* **1980**, 126−128.
(18) Majima, T.; Pac, C.; Nakasone, A.; Sakurai, H. *J. Am. Chem. Soc.* **1981**, *103*, 4499−4508.

Table 1. Selected Features[a] of TTD and Its Radical Cation

	TTD			TTD$^{\bullet+}$					
	expt[b]	HF	B3LYP	UHF	ROHF	UMP2	BLYP	B3LYP	B3LYP (C_{2v})
N_1-C_2	1.470(7)	1.450	1.464	1.455	1.454	1.464	1.480	1.469	1.450, 1.478 (N_3-N_6)
N_1-C_{10}	1.450(7)	1.448	1.458	1.425	1.424	1.434	1.446	1.437	1.469, 1.491 (N_3-C_4)
C_9-C_{10}	1.534(8)	1.556	1.570	1.598	1.600	1.599	1.618	1.608	1.575, 1.542 (C_4-C_5)
N_1-N_8	2.905	2.785	2.825	2.738	2.733	2.766	2.796	2.771	2.913, 2.280 (N_3-N_6)
N_1-N_3	2.508	2.485	2.518	2.431	2.430	2.462	2.491	2.468	2.433
$N_1C_2N_3$	116.9(3)	117.9	118.6	113.3	113.4	114.5	114.6	114.3	112.4
$N_1C_{10}C_9$	118.9(2)	115.1	115.5	113.6	113.5	114.0	114.1	113.9	117.1, 104.3 ($N_3C_4C_5$)
$C_2N_1C_{12}$	119.3(3)	115.3	115.0	118.4	118.3	117.5	117.4	117.6	108.9, 118.1 ($C_2N_3C_{11}$)
$C_2N_1C_{10}$	111.9(2)	115.1	114.9	115.5	115.6	115.5	115.5	115.6	116.5, 120.3 ($C_2N_3C_4$)
$\sum N_1$[c]	343.1	345.5	344.7	349.4	349.5	348.5	349.1	348.8	341.9, 358.7 (ΣN_3)
ρ (N_1)[d]				0.31	0.20	0.31	0.23	0.24	0.04, 0.48
energy[e]		−529.99694	−533.43777	−529.73675	−529.73675	−531.46807	−5.39467[f]	−533.20137	−533.17114

[a] Bond lengths in Å, bond angles in degrees; for numbering see Figure 2; D_{2d} symmetry unless noted otherwise; all computations used the 6-31G* basis set, except for BLYP/DZP. [b] X-ray data from ref 11. [c] Sum of bond angles around nitrogen. [d] Spin density on each of the equivalent nitrogens. [e] Energy in hartree. [f] Bonding energy relative to the fragments (frozen core).

a 3 mL solution can take thousands of 2 mJ laser pulses without noticeable degradation.

Resonance Raman Spectra. Resonance Raman spectra of TTD$^{\bullet+}$ in acetonitrile solution at room temperature were measured with the setup described.[19] Solutions of 5 mM TTD in acetonitrile were used. The radical cation was produced via photoionization at 248 nm (Lambda Physik LPX 220i excimer laser; 20 ns pulse width, ca. 6 mJ per pulse). The probe wavelength was 550 nm, in resonance with the main absorption band of the radical cation. A notch filter at the same wavelength (SN550) was used to filter the Raleigh scattering. The sample was refreshed after ca. 2000 excimer laser shots.

Calculations. Ab initio quantum chemical calculations of optimized geometries and harmonic force fields of radical cations were performed with a number of methods and programs. With the Gaussian94[20] and Gaussian98 programs,[21] unrestricted Hartree−Fock (UHF), second-order Møller−Plesset (MP2), and hybrid HF/density functional B3LYP calculations were carried out. The standard 6-31G* basis set was used. Single-point calculations of the vertically excited states of TTD$^{\bullet+}$ at the D_{2d} and C_{2v} optimized geometries were performed using time-dependent DFT[22] with the B3LYP functional. Self-consistent field calculations of the potential energy surface of the $^2A_1$ excited state of TTD$^{\bullet+}$ (D_{2d} symmetry only) were performed with the ROHF method implemented in Gamess,[23] and with BLYP density functional calculations using ADF (version 2.3)[24−26] with a double-ζ + polarization (DZP) basis set. Unfortunately, we did not have a computer program available which can handle non-Abelian point groups and contains the B3LYP functional. Complete active space SCF calculations were also attempted, but because the electron correlation in radical cations of this type is purely dynamical in nature,[27] inclusion of virtual orbitals in the active space had no effect on the wave function, and the results were identical to those obtained with ROHF.

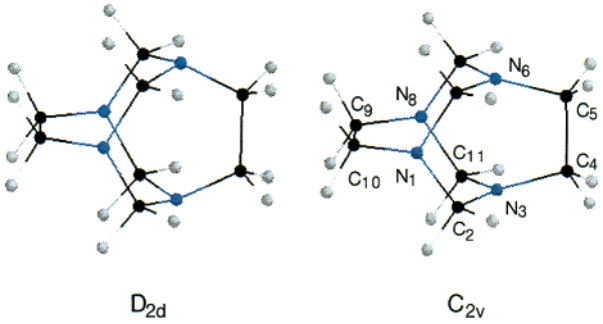

Figure 2. Calculated D_{2d} and C_{2v} structures (with numbering scheme) (B3LYP/6-31G*) of TTD$^{\bullet+}$.

3. Results and Discussion

Computed Molecular Structures. B3LYP/6-31G* calculations of the neutral TTD molecule reproduce the X-ray results rather well (Table 1). The D_{2d} structure appears as a true minimum. HF/6-31G* and MP2/6-31G* predict "twisted" minima of S_4 symmetry, in agreement with our recent experimental results, as discussed elsewhere.[16,28] Using the UB3LYP/6-31G* method, we could locate two minima on the potential energy surface of the ground state of the radical cation TTD$^{\bullet+}$: a highly symmetrical D_{2d} structure and a C_{2v} structure. These structures are shown in Figure 2, and relevant features are listed in Table 1. Geometry optimizations starting from asymmetric structures led to (near-)D_{2d} structures. Calculations at the UHF/6-31G* level showed wave function instability for both the C_{2v} and D_{2d} structures. After full optimization of the wave function, the spin density was localized on one nitrogen, even when the molecular geometry had D_{2d} symmetry. Despite this characteristic problem of HF theory,[29] the structures predicted within the constraint of D_{2d} symmetry are not very different from the B3LYP structure.

(19) Balakrishnan, G.; Keszthelyi, T.; Wilbrandt, R.; Zwier, J. M.; Brouwer, A. M.; Buma, W. J. *J. Phys. Chem. A* **2000**, *104*, 1834−1841.
(20) Frisch, M. J.; Trucks, G. W.; Schlegel, H. B.; Gill, P. M. W.; Johnson, B. G.; Robb, M. A.; Cheeseman, J. R.; Keith, T.; Petersson, G. A.; Montgomery, J. A.; Raghavachari, K.; Al-Laham, M. A.; Zakrzewski, V. G.; Ortiz, J. V.; Foresman, J. B.; Cioslowski, J.; Stefanov, B. B.; Nanayakkara, A.; Challacombe, M.; Peng, C. Y.; Ayala, P. Y.; Chen, W.; Wong, M. W.; Andres, J. L.; Replogle, E. S.; Gomperts, R.; Martin, R. L.; Fox, D. J.; Binkley, J. S.; Defrees, D. J.; Baker, J.; Stewart, J. J. P.; Head-Gordon, M.; Gonzalez, C.; Pople, J. A. *Gaussian 94*, Revision D.1, Revision B.2; Gaussian, Inc.: Pittsburgh, PA, 1995.
(21) Frisch, M. J.; Trucks, G. W.; Schlegel, H. B.; Scuseria, G. E.; Robb, M. A.; Cheeseman, J. R.; Zakrzewski, V. G.; J. A. Montgomery, J.; Stratmann, R. E.; Burant, J. C.; Dapprich, S.; J. M. Millam; Daniels, A. D.; Kudin, K. N.; Strain, M. C.; Farkas, O.; Tomasi, J.; Barone, V.; Cossi, M.; Cammi, R.; Mennucci, B.; Pomelli, C.; Adamo, C.; Clifford, S.; Ochterski, J.; Petersson, G. A.; Ayala, P. Y.; Q. Cui; Morokuma, K.; Malick, D. K.; Rabuck, A. D.; Raghavachari, K.; Foresman, J. B.; Cioslowski, J.; Ortiz, J. V.; Stefanov, B. B.; Liu, G.; Liashenko, A.; Piskorz, P.; Komaromi, I.; Gomperts, R.; Martin, R. L.; Fox, D. J.; Keith, T.; Al-Laham, M. A.; Peng, C. Y.; Nanayakkara, A.; Gonzalez, C.; Challacombe, M.; Gill, P. M. W.; Johnson, B.; Chen, W.; Wong, M. W.; Andres, J. L.; Gonzalez, C.; Head-Gordon, M.; Replogle, E. S.; Pople, J. A. *Gaussian 98*; Gaussian, Inc.: Pittsburgh, PA, 1998.
(22) Stratmann, R. E.; Scuseria, G. E.; Frisch, M. J. *J. Chem. Phys.* **1998**, *109*, 8218−8224.
(23) Schmidt, M. W.; Baldridge, K. K.; Boatz, J. A.; Elbert, S. T.; Gordon, M. S.; Jensen, J. J.; Koseki, S.; Matsunaga, N.; Nguyen, K. A.; Su, S.; Windus, T. L.; Dupuis, M.; Montgomery, J. A. *J. Comput. Chem.* **1993**, *14*, 1347−1363.
(24) Baerends, E. J.; Ellis, D. E.; Ros, P. *Chem. Phys.* **1973**, *2*, 41.
(25) Versluis, L.; Ziegler, T. *J. Chem. Phys.* **1988**, *88*, 322.
(26) te Velde, G.; Baerends, E. J. *J. Comput. Phys.* **1992**, *99*, 84.
(27) Brouwer, A. M.; Zwier, J. M.; Svendsen, C.; Mortensen, O. S.; Langkilde, F. W.; Wilbrandt, R. *J. Am. Chem. Soc.* **1998**, *120*, 3748−3757.
(28) Zwier, J. M. Ph.D. Thesis, University of Amsterdam, 2000.

For neutral TTD, MP2/6-31G* calculations in contrast to B3LYP correctly reproduce the symmetry lowering to S_4, but for the radical cation they also predict a D_{2d} structure to be a true minimum. The computed harmonic frequency of the a_2 torsional vibration, which distorts the molecule to S_4 symmetry, however, is only 46 cm^{-1} (80 cm^{-1} with B3LYP). The fluorescence excitation study[16] shows that the lowest excited Rydberg state of TTD, which on the basis of previous experience[19,30] may be expected to be very similar to the radical cation, definitely has a single D_{2d} minimum.

Although our calculations confirm the possibility of a C_{2v} minimum,[13] the D_{2d} structure is 19 kcal/mol lower in energy at the B3LYP/6-31G* level. Even at the HF level, which strongly favors charge localization even at the expense of symmetry breaking of the electron density distribution, the D_{2d} structure is the most stable. Density functional methods have a tendency to predict a too large extent of delocalization, especially in weakly coupled systems,[29,31,32] but in the present case the computational result on its own forms strong evidence in favor of the D_{2d} structure.

Selected geometrical parameters for neutral TTD and both radical cation structures are given in Table 1. Complete structural data are given in the Supporting Information. The long C−C bond in the D_{2d} structure is a typical result of 1,4-through-bond interaction between the nitrogen lone pairs.[2,27] In the C_{2v} structure, the positive charge is localized on one NCH_2CH_2N fragment. The 1,4-N−N distance decreases from 2.90 Å in the neutral molecule to 2.28 Å in the radical cation. This distance is similar to that found experimentally[10] and computationally[33] for **3**$^{\bullet+}$, which has a 3e-σ-bond between the nitrogens. The other 1,4-N−N distance is slightly larger than that in the D_{2d} neutral structure. In the neutral fragment, the C−C bond is similar to that in the neutral molecule; in the charged fragment it is shortened by 0.03 Å.

The structural changes upon ionization in TTD are relatively small. The energy gained when the radical cation structure is changed from that of the neutral molecule (computed vertical ionization potential $IP_v = 6.62$ eV) to the optimized geometry is 0.19 eV (adiabatic ionization potential $IP_a = 6.43$ eV). On the potential energy surface of the neutral molecule, the corresponding relaxation energy is 0.20 eV.

Vibrational frequencies of TTD$^{\bullet+}$ were calculated with the B3LYP/6-31G* method for the C_{2v} and the D_{2d} minima. As shown below, the latter explains the experimentally observed Raman spectrum better than the former. With BLYP/DZP and ROHF/6-31G*, we computed the force constants of the $^2B_2$ ground state and the gradient and the Hessian matrix of the $^2A_1$ excited state. These results, and those of the calculations of EPR and optical spectra, will be presented below in connection with the discussion of the experimental results.

EPR Spectra. TTD and its deuterated derivatives were oxidized with tris(4-bromophenyl)aminium hexachloroantimonate in CH_2Cl_2. The corresponding EPR spectra together with their simulations and ENDOR spectra are displayed in Figure 3. In all cases, a matching agreement is found between the experimental spectra and the calculated counterparts: for **2-d$_8$a**$^{\bullet+}$ the ENDOR spectrum reveals a ^{1}H hfc of 0.740 mT and a ^{2}H hfc of 0.008 mT (corresponding to a ^{1}H hfc of 0.069 mT). A matching simulation of the experimental EPR spectrum is established with an additional ^{14}N hfc of 0.345 mT for four equivalent N nuclei. Analogous hyperfine data hold for **2-d$_8$b**$^{\bullet+}$: a ^{1}H hfc of 0.069 mT and a ^{2}H hfc of 0.121 mT (conforming with the ^{1}H hfc of 0.740 mT). Thus, it is borne out that the hfc's of the protons in the ethylene bridge (H_b) carry a substantially higher portion of the spin population than those in the methylene bridge (H_a). The two differing spin populations in the methylene and ethylene bridges are corroborated by the simulation of the EPR signal of **2-d$_{16}$**$^{\bullet+}$. For all simulations, ^{14}N hfc's of four equivalent N atoms of ca. 0.35 mT were utilized. A corresponding set of hyperfine data was also used for the simulation of the EPR spectrum obtained after oxidation of parent TTD (**2**). Again, the agreement between the calculated and the experimental EPR spectra is excellent. Conspicuously, these data are at variance with those formerly published (^{1}H, 0.768; ^{1}H, 0.414; ^{14}N, 0.709 mT). It must be borne in mind, however, that the former study of the radical cation of **2** did not make use of the ENDOR technique and the deuterated derivatives were not available. The experimental hyperfine data agree very well with those calculated for the D_{2d} structure (see Figure 4). The ^{14}N hfc's are also appropriate indicators for the type of interaction between nitrogen centers. Therefore, a short description of the factors which bias the nature of ^{14}N hfc's is presented before a specific description of TTD$^{\bullet+}$ will be given.

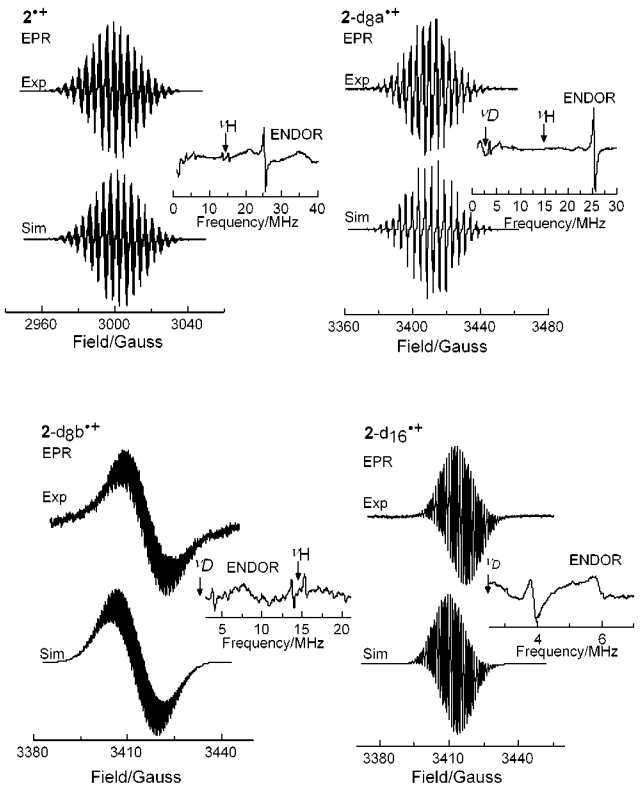

Figure 3. EPR/ENDOR spectra of **2**$^{\bullet+}$ and its deuterated derivatives **2-d$_8$a**$^{\bullet+}$, **2-d$_8$b**$^{\bullet+}$, and **2-d$_{16}$**$^{\bullet+}$ together with the EPR simulations.

(29) Bally, T.; Borden, W. T. In *Reviews in Computational Chemistry*; Lipkowitz, K. B., Boyd, D. B., Eds.; VCH: New York, 1999; Vol. 13, pp 1−97.
(30) Zwier, J. M.; Wiering, P. G.; Brouwer, A. M.; Bebelaar, D.; Buma, W. J. *J. Am. Chem. Soc.* **1997**, *119*, 11523−11533.
(31) Bally, T.; Sastry, G. N. *J. Phys. Chem. A* **1997**, *101*, 7923−7925.
(32) Sodupe, M.; Bertran, J.; Rodriguez-Santiago, L.; Baerends, E. J. *J. Phys. Chem. A* **1999**, *103*, 166−170.
(33) Zwier, J. M.; Wichers Hoeth, J.; Brouwer, A. M. *J. Org. Chem.* **2001**, *66*, 466−473.

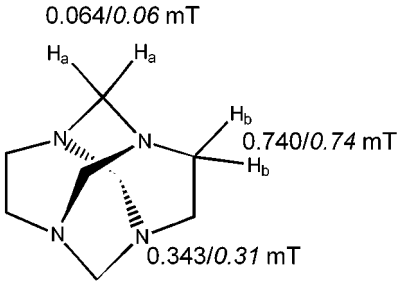

Figure 4. Experimental and calculated (UB3LYP/6-31G*, in italics) hfc's of $\mathbf{2}^{\bullet+}$.

Chart 2

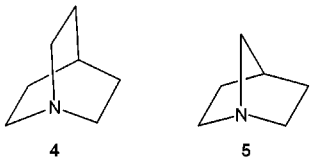

Geometry, Interactions, and the ^{14}N hfc's—An Excursion. Detailed information about the structure of nitrogen-centered radical cations can be deduced from their EPR spectra: the ^{14}N isotropic hyperfine coupling constants (hfc's) manifest a remarkable dependence upon three factors. In first respect the ^{14}N hfc depends on the pyramidalization or, in other words, hybridization at the nitrogen center. This is illustrated by the following examples. Trialkylamine radical cations generally have a ^{14}N hfc of ca. 2 mT. In these cases, a planar geometry around the N atom is achieved on the hyperfine time scale, and the unpaired electron resides in a "pure p_z-type" orbital. If the flattening at the N atom is hindered, e.g., when the amine is part of a rigid system, the s character of the singly occupied orbital and, in parallel, the ^{14}N hfc increases. For example, [1-azabicyclo[2.2.2]octane]$^{\bullet+}$ (**4**, Chart 2) has a ^{14}N hfc of 2.51 mT,[34] and in the even stronger pyramidalized radical cation of 1-azabicyclo[2.2.1]heptane (**5**) it increases to 3.02 mT. In both cases, the changes of the ^{14}N hfc are not connected to an altered amount of electron delocalization but depend only on the amount of pyramidalization. Analogous relationships have been established for hydrazine[35−37] and diazene[37] radical cations.

In *di*amines such as **3**, not only pyramidalization but also the relative orientation of the lone pairs and contributions of the connecting chains direct the size of the ^{14}N hfc.[38,39] For the diamine radical cations discussed in this contribution, two arrangements are to be distinguished: "out,out", where the nitrogen lone pairs are oriented away from two facing nitrogen atoms, and "in,in", where the lone pairs are directed toward each other. If we define the angle γ as the average of the angles N,N,X (X = substituent, Figure 5), $\gamma > 90°$ represents "in,in" and $\gamma < 90°$ "out,out". A planar arrangement of the two amino moieties is characterized by $\gamma = 90°$. Different rotamers, i.e., staggered or eclipsed conformations, are not of importance in this context.

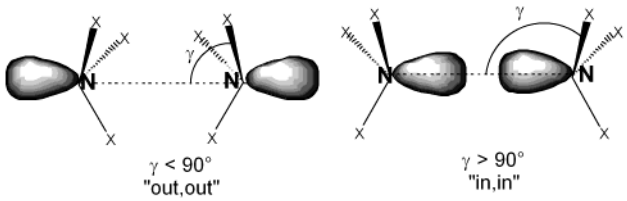

Figure 5. Two isomers of the X_3N- - -NX_3 fragment in (bicyclic) diamines and definition of the angle γ.

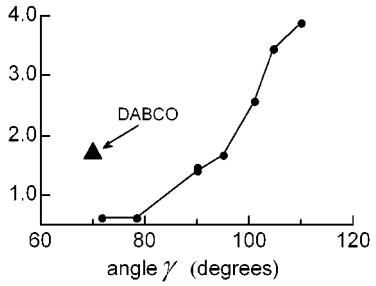

Figure 6. Geometry versus ^{14}N hyperfine coupling constants.

Chart 3

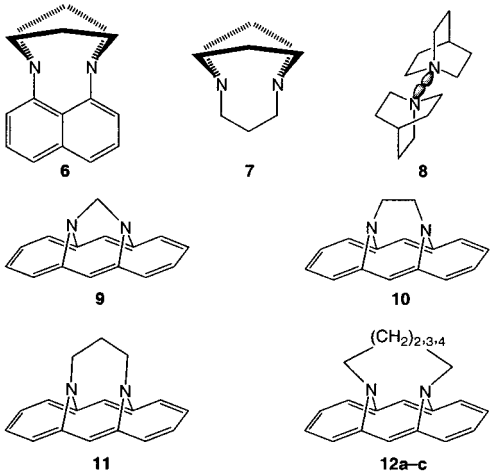

It has been shown that diamines such as **3** and **6**−**12** (Chart 3) form rather persistent radical cations.[39−44] The ^{14}N hfc's derived from the EPR spectra of $\mathbf{3}^{\bullet+}$ and $\mathbf{6}^{\bullet+}$−$\mathbf{12}^{\bullet+}$ follow a systematic route.

In Figure 6, the ^{14}N hfc's of the radical cations are plotted vs the angle γ. Although the spin population at the two N atoms remains virtually constant, the ^{14}N hfc's range from ca. 0.6 to 3.8 mT. Evidently, as the angle γ increases, the ^{14}N hfc grows, i.e., the stronger the "in,in" pyramidalization, the larger becomes the ^{14}N hfc. In diiminoannulene **9**, the ^{14}N hfc is 0.621 mT, whereas it grows to 2.56 mT in **12c**.[41] The ^{14}N hfc further increases to 3.6 and 3.8 mT in 1,5-diazabicyclo[4.4.4]tetradecane ($\mathbf{3}^{\bullet+}$)[10,42] and in the quinuclidine dimer ($\mathbf{8}^{\bullet+}$),[44] respectively (Figure 6). The correlation between the hfc and the geometry at the N atoms holds for all diamines, and both for "in,in" and "out,out" pyramidalization where a n$_-$-type orbital is singly

(34) Danen, W. C.; Rickard, R. C. *J. Am. Chem. Soc.* **1975**, *97*, 2303−2304.
(35) Neugebauer, F. A.; Weger, H. *J. Phys. Chem.* **1978**, *82*, 1152−1157.
(36) Nelsen, S. F.; Blackstock, S. C.; Yumibe, N. P.; Frigo, T. B.; Carpenter, J. E.; Weinhold, F. *J. Am. Chem. Soc.* **1985**, *107*, 143−149.
(37) Gescheidt, G.; Lamprecht, A.; Ruechardt, C.; Schmittel, M. *Helv. Chim. Acta* **1991**, *74*, 2094−2099.
(38) Alder, R. W.; Heilbronner, E.; Honegger, E.; McEwen, A. B.; Moss, R. E.; Olefirowicz, E.; Petillo, P. A.; Sessions, R. B.; Weisman, G. R.; White, J. M.; Yang, Z. Z. *J. Am. Chem. Soc.* **1993**, *115*, 6580−6591.
(39) Alder, R. W. *Tetrahedron* **1990**, *46*, 683−713.
(40) Gerson, F.; Gescheidt, G.; Buser, U.; Vogel, E.; Lex, J.; Zehnder, M.; Riesen, A. *Angew. Chem* **1989**, *101*, 938−940.
(41) Gerson, F.; Gescheidt, G.; Knoebel, J.; Martin, W. B. J.; Neumann, L.; Vogel, E. *J. Am. Chem. Soc.* **1992**, *114*, 7107−7115.
(42) Kirste, B.; Alder, R. W.; Sessions, R. B.; Bock, M.; Kurreck, H.; Nelsen, S. F. *J. Am. Chem. Soc.* **1985**, *107*, 2635−2640.
(43) Alder, R. W.; Sessions, R. B. *J. Am. Chem. Soc.* **1979**, *101*, 3651−3652.
(44) Dinnocenzo, J. P.; Banach, T. E. *J. Am. Chem. Soc.* **1988**, *110*, 971−973.

Chart 4

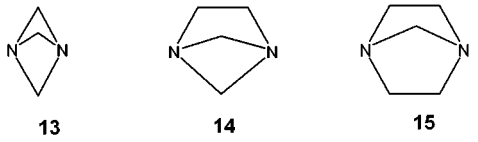

Chart 5

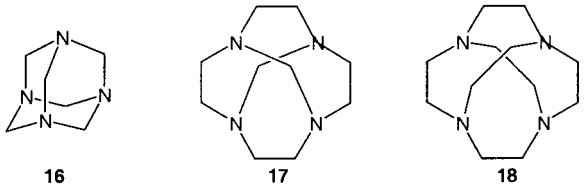

occupied and in some cases even a σ N−N bond has been established experimentally by X-ray analysis.[9,10,39−41,44,45] The model system $[H_3N\text{- - -}NH_3]^{\bullet+}$ presents the same dependence of the pyramidalization at nitrogen vs the ^{14}N hfc (see Supporting Information). The only diamine radical cation which does *not* obey this rule is DABCO (**1**$^{\bullet+}$), because "through-bond" interaction via ethylene bridges dominates, leading to the inversion in the sequence of the frontier orbitals (the singly occupied orbital is of n_+ type).[46]

Before switching to tetraamines, let us consider confined bicyclic diamines, closely related to DABCO (**2**). What is the influence of methylene or ethylene bridges in polycyclic diamines? To this end, we inspect structures **13**, **14**, and **15**. None of the corresponding radical cations has been reported; therefore, we concentrate on calculated data (calculations on the B3LYP/6-31G* level of theory are well established for their reliability, see above and refs 47 and 48).

The radical cation of **13** (Chart 4) shows a (calculated) ^{14}N hfc of 0.595 mT, in very good agreement with the related radical cation of **9** (0.621 mT); here the nitrogen lone pairs are oriented "out,out", and the pyramidalization angle γ is ca. 60°. If one of the methylene bridges is replaced by an ethylene bridge as in **14**$^{\bullet+}$, the ^{14}N hfc remains almost constant (0.596 mT), and even the presence of two ethylene bridges (**15**$^{\bullet+}$, ^{14}N hfc, 0.770 mT) still produces an n_--type singly occupied orbital. Only with three ethylene bridges (DABCO), the ^{14}N hfc increases to 1.490 mT (experimental, 1.41 mT), and the SOMO symmetry changes to n_+ type; i.e., through-bond coupling of the three ethylene bridges becomes dominant.

Finally, the situation in TTD-related polycycles is examined. They can be regarded as "dimers" of the compounds **2** and **13**−**15**. Tetraazaadamantane **16** (Chart 5) possesses only methylene bridges, whereas in **18** the four nitrogen atoms are connected by ethylene units. Polycycle **17** has two ethylene and one methylene at each nitrogen, whereas TTD (**2**) carries two methylene and one ethylene at each N center. All four tetraazapolycycles constitute "out,out,out,out" systems in the neutral stage. This arrangement is retained in the relatively rigid **16**$^{\bullet+}$. The pyramidalization at two of the four N atoms is flattened, with an almost unchanged geometry at the remaining nitrogens. As a consequence, the spin becomes localized at the two more planar N centers (^{14}N hfc, 1.08 mT (2 N), 0.02 mT (2 N); calcd). Because only delocalized systems are of interest here, we do not further consider **16**$^{\bullet+}$. On the other hand, one-electron oxidation of the rather flexible molecules **17** and **18** yields radical cations adopting an "in,in,in,in" geometry with an almost planar arrangement at the N atoms. This causes the calculated ^{14}N hfc's of 0.60 and 0.75 mT for **17**$^{\bullet+}$ and **18**$^{\bullet+}$ to be considerably larger than those for **2**$^{\bullet+}$ (0.31 mT). In **17**$^{\bullet+}$ and **18**$^{\bullet+}$, two N atoms interact pairwise via the ethylene bridges by through-bond coupling and are interconnected by through-space communication. It is noteworthy that the ^{14}N hfc of the *tetra*amine **18**$^{\bullet+}$ (0.75 mT) is almost exactly one-half of that found for the *di*amine DABCO (**1**, 1.49 mT).

Structural Features of TTD$^{\bullet+}$ Derived from EPR. The singly occupied MO of **2**$^{\bullet+}$ has most of its density at the four equivalent nitrogen centers, but a considerable amount of electron density resides at the C−C bond in the ethylene bridges and is accordingly transferred to the adjacent protons. On the other hand, the methylene bridges lie close to the nodal planes of the π-type orbitals centered at the nitrogen atoms. Thus, a markedly lower amount of spin density resides on the protons of the methylene bridges. This explains why the hfc of H_b is much larger than that of H_a. Interestingly, the ^{1}H hfc for the latter is about twice as big as the ^{14}N hfc. This is unusual, since the hfc's of protons in β-positions to nitrogen radical centers generally are (at maximum) of the same size as the ^{14}N hfc's; e.g., in DABCO (**1**) the ^{14}N hfc is 1.7 mT and the ^{1}H is 0.73 mT, and in **9** (**10**) these values amount to 0.63 (0.61) and 0.15 mT, respectively.

What is the reason for this unusually small ^{14}N hfc? The N centers are pyramidalized. The average bond angle (Table 1) is 116° (120° corresponds to a planar arrangement), which implies a slight flattening compared to the neutral precursor (114.9° according to B3LYP/6-31G* and 114.4° according to the X-ray structure).[11] Still, the relative pyramidalization at the N centers is "out,out,out,out", and indeed the corresponding ^{14}N hfc of 0.34 mT represents about one-half of that established for "out,-out" *di*amines with dominating through-space interaction (**9**$^{\bullet+}$, **10**$^{\bullet+}$, **13**$^{\bullet+}$, **14**$^{\bullet+}$, and **15**$^{\bullet+}$). On the other hand, the peculiarly large hfc's of H_b reflect the through-bond contributions, similar to **1**$^{\bullet+}$.

Localized or Delocalized Molecular Structure of TTD$^{\bullet+}$. The experimental and computed hfc's, represented in Figure 4, are mutually consistent and further support the notion of a single D_{2d} energy minimum for TTD$^{\bullet+}$. In principle, however, it is possible that a similar agreement would be obtained if the EPR spectrum is attributed to two rapidly interconverting C_{2v} forms. If the reasonable assumption is made that the UB3LYP/6-31G* calculations give reliable estimates of hfc's,[47] then we may use the computed values for the C_{2v} structure. The ^{14}N hfc for the two (equivalent) nitrogens involved in the three-electron bond is computed to be 1.06 mT and for the remaining pair of distant N atoms amounts to −0.074 mT. If a fast exchange of spin density between these two pairs of nitrogens would occur, the average ^{14}N hfc should amount to 0.49 mT. This is at variance with the experimental value of the delocalized system (D_{2d}, experimental 0.35 mT, calculated 0.31 mT). Moreover, the ^{1}H hfc's would be equal to 0.75 mT for the methylene and 0.026 mT for the ethylene bridges, respectively; again, a clear differ-

(45) Honegger, E.; Yang, Z. Z.; Heilbronner, E.; Alder, R. W.; Moss, R. E.; Sessions, R. B. *J. Electron Spectrosc. Relat. Phenom.* **1985**, *36*, 297−304.
(46) Albright, T. A.; Burdett, J. K.; Whangbo, M.-H. *Orbital Interactions in Chemistry*; Wiley: New York, 1985.
(47) Batra, R.; Giese, B.; Spichty, M.; Gescheidt, G.; Houk, K. N. *J. Phys. Chem.* **1996**, *100*, 18371−18379.
(48) Gauld, J. W.; Eriksson, L. A.; Radom, L. *J. Phys. Chem. A* **1997**, *101*, 1352−1359.

ence from the D_{2d}-symmetric $\mathbf{2}^{\bullet+}$, where the assignment of the ^{1}H hfc's is established by the deuterated derivatives (Figure 4). Thus, the EPR results support a delocalized structure of $\mathbf{2}^{\bullet+}$.

Optical Absorption Spectra. Simultaneously with the EPR spectra, optical spectra of all samples were recorded. All isotopomers showed identical absorption spectra, as expected: a single band in the range 400−800 nm with a maximum at ca. 565 nm. The absorption spectrum of $TTD^{\bullet+}$ in CH_3CN produced via the cosensitization method is virtually identical, the maximum being at ca. 560 nm. Vertical excitation energies of $TTD^{\bullet+}$ were computed with the time-dependent DFT method. We have experienced that the B3LYP functional with the 6-31G* basis set can be used to estimate excitation energies of organic amine radical cations quite well.[33] The spectrum of $TTD^{\bullet+}$ was measured earlier by Haselbach and Bally[14] in an *n*-butyl chloride/isopentane matrix at low temperature. The maximum located at 559 nm ($\epsilon = 1260$ L mol^{-1} cm^{-1})[14] can be assigned to the transition from the $^2B_2$ cation ground state (D_{2d} geometry) to the $^2A_1$ state. The TDDFT-predicted absorption maximum is 536 nm (oscillator strength $f = 0.06$). A long-wavelength absorption band which corresponds to the vertical excitation to the degenerate ^2E excited state is located at 835 nm ($\epsilon = 580$ L mol^{-1} cm^{-1}) (TDDFT: 773 nm, $f = 0.02$).[14] This band was not detected in our experiments because of overlapping bands of the oxidant used in the SEOS experiments, and because it is outside the accessible spectral window of the gated OMA detector in the transient experiments. The computed excitation energies are only slightly higher than the experimental values, and the ratio of the oscillator strengths agrees qualitatively well with the experimentally found absorption coefficients. For the C_{2v} structure, the singly occupied orbital is located on the NCH_2-CH_2N fragment, having a through-space bond between the nitrogen atoms. Charge-transfer transitions involving the orbitals of the neutral NCH_2CH_2N moiety should occur in the IR (2669 nm, $f = 0.002$) and in the near-IR (913 nm, $f = 0.000$). An allowed transition in the visible is predicted at 529 nm ($f = 0.03$), corresponding to a local excitation in the charged NCH_2-CH_2N fragment. Clearly, the comparison of the calculated and observed electronic absorption spectra supports the notion that $TTD^{\bullet+}$ has a highly symmetric D_{2d} structure, not the localized C_{2v} structure.

Resonance Raman Spectra. Upon probing at 550 nm in resonance with the strongest electronic transition of $TTD^{\bullet+}$, the Raman spectra depicted in Figure 7 were obtained. Strong resonance enhancement of Raman transitions usually occurs only for totally symmetric modes.[49] Using the B3LYP/6-31G*-calculated a_1 vibrational frequencies for the D_{2d} structure, we could readily assign most bands in the spectra of the parent isotopomer. The frequencies computed for the C_{2v} structure, which has a larger number of totally symmetric modes, could explain the spectrum almost equally well, although a number of a_1 modes must then be assumed to have negligible Raman intensity, as shown in Table 2. The largest deviation in the frequencies calculated for the D_{2d} structure is in the predicted frequency of ν_6, which is overestimated by 26 cm^{-1}. This type of vibration, a twisting mode of the CH_2 groups in the (partially charged) NCH_2CH_2N fragment, is also found in other amine radical cations, and we have observed that its frequency is systematically rather strongly overestimated by B3LYP calculations. The vibrations at lower frequencies are clearly predicted much better for the D_{2d} structure than for the C_{2v} structure. The assignments in Table 2 are based on the computations for the D_{2d} structure and will be discussed in some detail below. Also included in Table 2 are the results obtained with BLYP/DZP, UMP2/6-31G*, and ROHF/6-31G* for the D_{2d} structure. The latter agree very well with experiment, despite the problems with wave function instability. All a_1 normal-mode frequencies of the four isotopomers of $TTD^{\bullet+}$ are listed in Table 3.

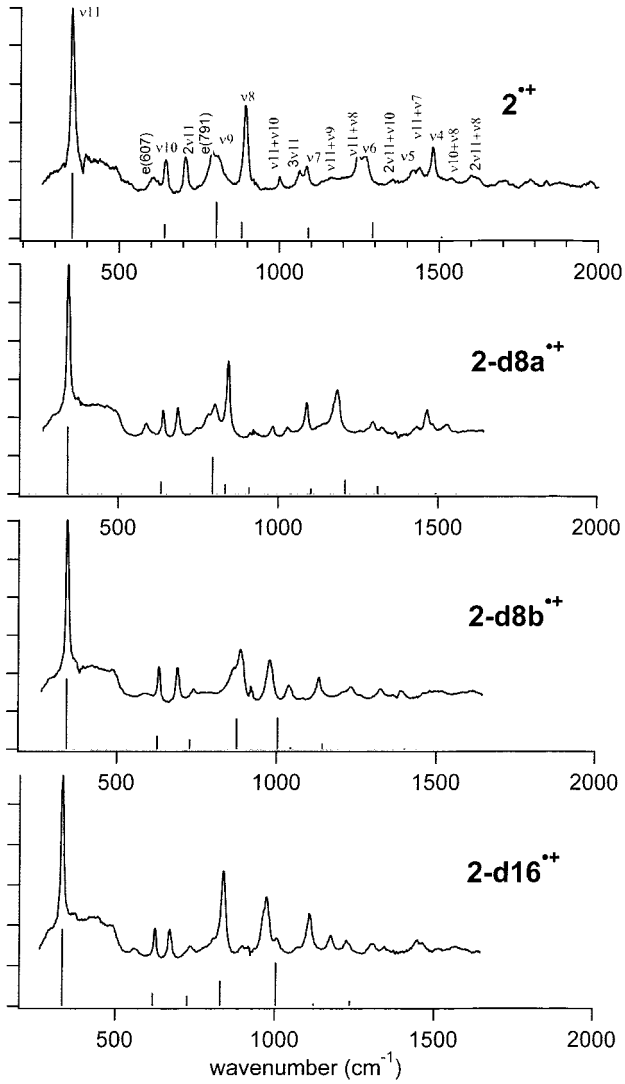

Figure 7. Resonance Raman spectra of radical cations of four TTD isotopomers: $\mathbf{2}^{\bullet+}$, $\mathbf{2\text{-}d_8a}^{\bullet+}$, $\mathbf{2\text{-}d_8b}^{\bullet+}$, and $\mathbf{2\text{-}d_{16}}^{\bullet+}$. The cations were formed by photoionization of TTD in acetonitrile at 248 nm (KrF excimer laser). The probe pulse was at 550 nm, in resonance with the main absorption transition. The relative resonance Raman intensities (stick diagrams) were computed on the basis of the ROHF excited-state gradient using eq 1; the frequencies used are from the ROHF/6-31G* calculation of the ground state, scaled ×0.90.

Discussion of the Resonance Raman Spectra. The appearance of the spectra of $TTD^{\bullet+}$ and the deuterated isotopomers is quite different from those of the radical cation of DABCO and related piperazine radical cations. The spectra are dominated by the intense band due to ν_{11}, a skeletal "breathing" vibration, and an unusually large number of overtones and combination bands involving ν_{11} is observed. The frequency of ν_{11} is only slightly influenced by substitution with deuterium. The C−N

(49) Myers, A. B. *Chem. Rev.* **1996**, *96*, 911−926.

Table 2. Experimental Resonance Raman and Computed Vibrational Wavenumbers (cm^{-1}) of $TTD^{\bullet+}$ [a]

exptl	assignment (D_{2d})	computed B3LYP,[b] D_{2d}	error D_{2d}	computed B3LYP,[b] C_{2v}	error C_{2v}	computed BLYP,[c] D_{2d}	BLYP error	computed ROHF,[d] D_{2d}	ROHF error	computed MP2,[e] D_{2d}	MP2 error
				314							
351	ν_{11}	353	−2	366	−15	358	−7	352	−1	345	6
				463							
607	e	619				618	−11			546	
644	ν_{10}	638	6	628	16	628	16	641	3	637	7
705	$2\nu_{11}$										
				736							
791	e	785				786	5			822	
810	ν_9	800	10	832	−22	769	41	803	7	825	−15
892	ν_8	886	6	912	−20	895	−3	882	10	889	3
				932							
999	$\nu_{11}+\nu_{10}$			1006	−7						
1064	$3\nu_{11}$										
1083	ν_7	1084	−1	1087	−4	1062	21	1091	−8	1110	−27
1161	$\nu_{11}+\nu_9$										
1246	$\nu_{11}+\nu_8$										
1268	ν_6	1294	−26	1253	15	1302	−34	1292	−24	1289	−21
				1339							
				1342							
1353	$2\nu_{11}+\nu_{10}$			1360	−7						
				1389							
1418	ν_5	1402	16			1414	4	1406	12	1396	22
1437	$\nu_{11}+\nu_7$										
1479	ν_4	1458	21	1468	11	1479	0	1469	10	1459	20
				1491							
	ν_3	1501		1500				1508		1500	
1538	$\nu_{10}+\nu_8$										
1601	$2\nu_{11}+\nu_8$										
average error[f]			4		−4		3		1		−1
standard deviation[f]			12.5		13.0		18.2		10.7		16.4

[a] 6-31G* basis set, except for BLYP; only totally symmetric normal modes reported, plus e-modes as necessary to explain experimental spectra. [b] B3LYP frequencies scaled ×0.974. [c] BLYP double-ζ + polarization basis set; frequencies scaled ×1.02. [d] ROHF frequencies scaled ×0.90. [e] MP2 frequencies scaled ×0.96. [f] a_1 fundamentals only.

Table 3. Experimental and Computed Vibrational Wavenumbers for Totally Symmetric Modes of $\mathbf{2}^{\bullet+}$ and Deuterated Isotopomers

	d_0		d_{8a}		d_{8b}		d_{16}	
	calcd	exptl	calcd	exptl	calcd	exptl	calcd	exptl
ν_{11}	353	351	343	343	345	344	335	334
ν_{10}	638	644	632	640	624	631	617	624
ν_9	800	810	793	802	731	740	728	735
ν_8	886	892	836	843	881	886	834	838
ν_7	1084	1083	911	n.o.	*1044*	n.o.	*894*	n.o.
ν_6	1294	1268	1313	1296	996	977	996	973
ν_5	1402	1418	*1197*	1185[b]	1397	1418	1220	1223
ν_4	1458	1479	1094	1089	1470	1479	1072	1067
ν_3	1501	n.o.	1491	n.o.	*1133*	1131	1114	1107
ν_2	3008	*c*	3010	*c*	2189	*c*	2186	*c*
ν_1	3016	*c*	2193	*c*	3014	*c*	2196	*c*

[a] Calculated wavenumbers (cm^{-1}) (B3LYP/6-31G*) scaled ×0.974; n.o. = not observed; numbers in italics indicate that the normal mode of the isotopomer is heavily mixed with other modes, and the correspondence to the normal mode of the parent $\mathbf{2}^{\bullet+}$ is not perfect. [b] Uncertain. [c] Outside spectral range observed experimentally.

bending mode, ν_{10}, also moderately changes upon deuteration. However, ν_9, which involves CH_2-CH_2 stretching, is strongly shifted to lower frequency for both $\mathbf{2\text{-}d_8b}^{\bullet+}$ and $\mathbf{2\text{-}d_{16}}^{\bullet+}$, which are deuterated on the CH_2-CH_2 positions. This vibration in $\mathbf{2\text{-}d_8a}^{\bullet+}$ hardly changes with respect to $\mathbf{2}^{\bullet+}$. For ν_8, which involves $N-CH_2-N$ bending, the reverse is happening. The position of ν_8 in $\mathbf{2\text{-}d_8b}^{\bullet+}$ is not changed, whereas this vibration in $\mathbf{2\text{-}d_8a}^{\bullet+}$ shifts 50 cm^{-1} to lower frequency. The computed frequency changes agree very well with those observed experimentally. Although the frequencies change substantially upon deuteration, the nature of these modes does not change much. In contrast, modes ν_7 to ν_4 all involve $N-CH_2-N$ and/or CH_2-CH_2 bending or twisting, and these modes strongly change character upon deuteration.

Most bands in the resonance Raman spectra can be explained using a_1 fundamental and combination bands, but some bands must be due to vibrations of different symmetry. This is perhaps not surprising, because vibronic interactions between the resonant $^2B_2$ excited state and the lower lying ^2E state are likely to exist. The most pronounced band, which cannot be due to a totally symmetric vibration (even if C_{2v} symmetry would be assumed), is the transition which is found at 607 cm^{-1} in $\mathbf{2}^{\bullet+}$ and which shifts to lower frequency upon deuteration. This band is probably due to an e vibration calculated at 619 cm^{-1} for $\mathbf{2}^{\bullet+}$. Other bands which must be attributed to non-totally symmetric modes also appear in some of the spectra, but their assignment is ambiguous.

Resonance Raman Intensities. The intensities of the peaks in a resonance Raman spectrum depend on the time evolution of the overlap of the vibrational wave packet created on the excited-state potential energy surface with the vibrational wave functions of the ground state. The resonance Raman spectrum (and the optical absorption spectrum) can be calculated using wave packet propagation on the excited-state surface.[49−52] Thus, in addition to the already available information of the ground-state surface, in terms of equilibrium geometry and harmonic force constants, we need a model of the excited-state surface.

(50) Heller, E. J. *Acc. Chem. Res.* **1981**, *14*, 368−375.
(51) Heller, E. J.; Sundberg, R. L.; Tannor, D. *J. Phys. Chem.* **1982**, *86*, 1822−1833.
(52) Tannor, D. J.; Heller, E. J. *J. Chem. Phys.* **1982**, *77*, 202−218.

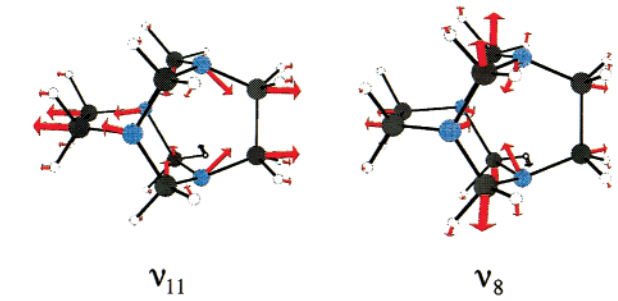

Figure 8. Normal mode displacements for ν_{11} and ν_8, which correspond to the most intense bands in the resonance Raman spectra of $TTD^{\bullet+}$.[55]

Although the quantum chemical methods used in this work cannot be expected to perform as well for the excited-state potential energy surface as they do for the ground state, in related cases we have been able to obtain highly satisfactory calculations of resonance Raman intensities using simple DFT calculations of excited states.[19,27,53]

In addition to the full time domain calculation, for which one needs the gradient and Hessian matrix of the excited-state surface at the ground-state geometry, or the optimized geometry and the Hessian calculated at that geometry, some simpler approximations have proven useful. Negri et al. proposed eq 1,[54] in which the relative intensities I_j are calculated from the dimensionless displacements obtained simply from the gradient vector **g** on the excited-state surface, with the assumption that the normal modes $\mathbf{L}_j$ and frequencies ν_j are the same in ground and excited states. **M** is the diagonal matrix of atomic masses.

$$I_j \sim (\mathbf{g}\mathbf{M}^{-1/2}\mathbf{L}_j\nu_j^{-3/2})^2 \qquad (1)$$

Using eq 1, we estimated the resonance Raman intensities by employing the normal modes and excited-state gradient calculated using the ROHF/6-31G* method. The results have been included in Figure 7. Evidently, the modeling is not perfect, but at least it is clear that the breathing mode ν_{11} gives the most intense band in the spectra of all isotopomers. Inspection of the orbitals occupied in the $^2B_2$ and $^2A_1$ states shows that upon excitation an expansion of the cage (increased antibonding interactions between the ethylenediamine moieties through space) and elongation of the C−C bonds (less σ bonding contribution) should be expected. The normal modes 11 and 8 (corresponding to the second most intense band in the spectra) are shown in Figure 8.

As mentioned above, TDDFT calculations for the C_{2v} structure of $TTD^{\bullet+}$ predict an absorption band near 530 nm. The transition in that case, however, is a one-electron excitation from the lowest of the "lone pair" orbitals located in the charged fragment, to the SOMO in the same fragment. C−C stretching and nitrogen pyramidalization modes would then be the most strongly resonance enhanced transitions, as in the case of DABCO.[19]

Orbital Interactions in TTD. Inspection of the frontier MOs (Figure 1) reveals that the orbital symmetries with respect to the symmetry planes are symmetric < antisymmetric < symmetric. In each NCH_2CH_2N fragment, the situation is like in DABCO (**1**). The magnitude of the through-bond splitting, as measured via the experimental ionization potentials, is 1.27 eV (A_1−E) or 0.88 eV (E−B_2). The interaction *between* the two diamine fragments arises from 1,3-interactions through space: in the A_1 MO the interaction is bonding (all lone pair orbitals in-phase), in the E MO there is no net through-space coupling between the diamine units, and in the B_2 MO the 1,3-interactions are antibonding. While the through-bond interaction within the diamine fragments gives rise to the typical structural feature of an elongated C−C bond and high spin density on the protons (H_b) in the ethylene bridges, the through-space interaction is reflected in the dominance of the breathing mode ν_{11} in the resonance Raman spectrum.

4. Concluding Remarks

The combination of theoretical calculations, optical spectroscopy, resonance Raman, and EPR measurements has revealed a consistent picture of structure of the TTD radical cation on different dynamical time scales. Upon oxidation, TTD undergoes relatively small geometrical changes, and the radical cation can be identified by a characterictic electronic absorption spectrum which is virtually independent of the procedure of generation (marginal solvent and/or counterion effects). The uncomplicated synthesis, the low ionization potential, and the small reorganization energy together with the straightforward identification of the corresponding radical cation could make TTD an attractive reagent in electron-transfer studies.

Acknowledgment. Financial support from the Swiss National Science Foundation and Ciba Speciality Chemicals is gratefully acknowledged. S.F.N. thanks the National Science Foundation for partial financial support under Grant CHE-8415077. The Netherlands Organization for Scientific Research (Nederlandse Organisatie voor Wetenschappelijk Onderzoek, NWO) supported this work with travel grants to J.M.Z.

Supporting Information Available: Cartesian coordinates of all relevant computed structures; calculations on the H_3N- - -NH_3 radical cation (PDF). This material is available free of charge via the Internet at http://pubs.acs.org.

JA016999N

(53) Brouwer, A. M.; Svendsen, C.; Mortensen, O. S.; Wilbrandt, R. *J. Raman Spectrosc.* **1998**, *29*, 439−445.
(54) Negri, F.; Orlandi, G.; Zerbetto, F.; Zgierski, M. Z. *J. Chem. Phys.* **1995**, *103*, 5911−5918.
(55) Bode, B. M.; Gordon, M. S. *J. Mol. Graphics Modell.* **1998**, *16*, 133−138.